THE JOURNAL OF PHYSICAL CHEMISTRY B

Article

pubs.acs.org/JPCB

Imide Photodissociation Investigated by X-ray Absorption Spectroscopy

Phillip S. Johnson,[†] Peter L. Cook,[‡] Xiaosong Liu,[§] Wanli Yang,[§] Yiqun Bai,[⊥] Nicholas L. Abbott,[⊥] and F. J. Himpsel*,[†]

[†]Department of Physics, University of Wisconsin−Madison, 1150 University Avenue, Madison, Wisconsin 53706, United States

[‡]Natural Sciences Department, University of Wisconsin−Superior, Belknap and Catlin, Superior, Wisconsin 54880, United States

[§]Advanced Light Source, Lawrence Berkeley National Laboratory, 1 Cyclotron Road, Berkeley, California 94720, United States

[⊥]Department of Chemical and Biological Engineering, University of Wisconsin−Madison, 1415 Engineering Drive, Madison, Wisconsin 53706, United States

Supporting Information

ABSTRACT: X-ray absorption spectroscopy is used to investigate the photodissociation of the imides PMDI (pyromellitic diimide) and SSMCC (sulfosuccinimidyl 4-(*N*-maleimidomethyl) cyclohexane-1-carboxylate). PMDI contains only one type of imide, and its photodissociation can be explained by a simple conversion from imide to a mix of imine and nitrile after desorption of the oxygens from the imide. SSMCC contains two different imides. One reacts like PMDI, the other in a more complex multistep process. Eventually, N_2 is formed in the bulk of the sample at high radiation density. The sequence of reactions is inferred from the π^* peaks in total electron yield and fluorescence yield absorption spectra at the N 1s and O 1s edges. First-order rate equations are used to model the evolution of the peak areas versus radiation dose.

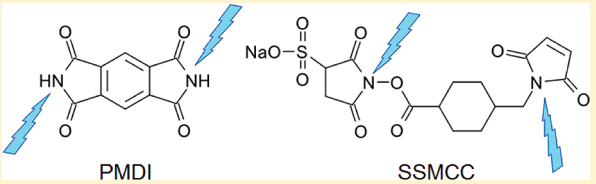

INTRODUCTION

The effect of irradiation on imides is a topic of continuing research, with applications in numerous fields. In particular, the effects of proton,[1,2] electron,[3] neutron, ion,[4] and gamma[5] irradiation on the properties of polyimide films have been investigated for their use in spacecraft and other applications requiring stability against temperature, penetration of aqueous solutions, and radiation. The photodissociation of imides by ionizing radiation is of interest because of their potential in organic dye-sensitized solar cells.[6] Imides also see use as linkers for protein attachment and for functionalizing surfaces for use in biosensors, DNA microarrays, and protein chips.[7,8] Polyimides are common insulators in microelectronics; they have been used in organic light-emitting diodes for their photoluminescent[9] and fluorescent[10] properties, and they are studied as models for fragmentation or other reactions of photoactive biomolecules.[11,12] Buffed polyimide is used to orient liquid crystals in flat panel displays.[13,14] Self-assembled monolayers containing imides are used for various nanotechnology applications.[15]

Changes in X-ray absorption spectra have been used before to study radiation damage in amino acids[16,17] and polymers (particularly as the damage appears in soft X-ray microscopy[18−20]). Others have investigated dissociation processes using low-energy electrons,[21] collision-induced dissociation,[22−27] electrospray ionization,[28,29] and matrix-assisted laser desorption ionization (MALDI).[30−32] This work uses imides as model systems for determining the mechanism and products of imide photodissociation using near edge X-ray absorption fine structure (NEXAFS) spectroscopy to provide element- and bond-specific insight into the changes in bonding as a function of radiation dose.

Recently, the dissociation of the amide bond under irradiation by soft X-rays was investigated.[33] A universal mechanism was found in a large variety of peptides, proteins, and polyamides using X-ray absorption spectroscopy at the C, N, and O 1s edges. First, oxygen is desorbed from the amide bond. This leaves two options for the H atom attached to the amide N to rearrange the broken carbonyl bond into a stable configuration. Migration of H to the carbonyl C leads to an imine, while migration to the C_α of the amino acid residue leads to a nitrile and thereby breaks the backbone of a protein or polyamide. A similar end product has been observed in the photodissociation of amino acids.[17]

Here, the spectroscopic method is extended to imides. Two imides are investigated: one as a simple model system, the other for extending the method to more complex reactions involving inequivalent imides. In pyromellitic diimide (PMDI), an aromatic, highly fluorescent polyimide,[10] the imides on either side of the molecule are identical and part of a conjugated π system. Sulfosuccinimidyl 4-(*N*-maleimidomethyl) cyclohexane-1-carboxylate (SSMCC) is a common linker for

Received: January 11, 2012
Revised: May 7, 2012
Published: May 17, 2012

immobilizing peptides on substrates.[7,8] Unlike PMDI, SSMCC has two distinct imides that differ in their surrounding structure (see Table 1). It is used as a model compound for testing the capability of X-ray absorption spectroscopy to analyze more complex molecules. One end of the molecule (labeled imide B1) resembles maleimide, and the other (labeled imide B2) resembles succinimide. The succinimidyl end is bonded to the carboxylate, and the maleimidyl end is bonded to a carbon.

Table 1. Structures of the Two Imides Examined

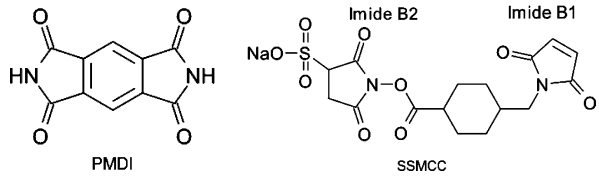

The presence of the two distinct imides in SSMCC is reflected in a radiation damage mechanism in which one imide (B2) is first converted into the other (B1) before both of them photodissociate. The later stage of the dissociation of imides resembles the photodissociation of amides and amino acids, in which oxygen is desorbed with subsequent formation of both imine and nitrile.[17,33] An additional dissociation product was observed at high irradiation intensity: the formation of N_2 trapped inside the organic matrix of SSMCC.

EXPERIMENTAL SECTION

Materials. The PMDI was purchased from Sigma-Aldrich and prepared by drop-casting a solution in ethanol onto a silicon wafer. The SSMCC was purchased from Pierce Biotechnology (Rockford, IL) and prepared by drop-casting a solution in phosphate-buffered saline (fluorescence yield measurements) or Milli-Q water (total electron yield measurements) onto a gold-coated silicon wafer. The solvents were confirmed to have minimal effect on the molecules' structure by comparing the spectra of the drop-cast samples to spectra of samples prepared by simply pressing either powder into carbon tape. Sample thickness was enough to be visible, much greater than the sampling depth.

Measurements. The X-ray absorption spectroscopy technique is described in our previous work on amides.[33] As done there, we focus on the N 1s absorption edge to obtain information that is specific to the N atom in the imide bond. The O 1s edge is used to detect O desorption from the C═O group. The C 1s edge is less informative because of the many other types of C atoms that are not related to the imide bond and, therefore, is not discussed here.

The photon energy for the total electron yield (TEY) spectra was calibrated at the N 1s and O 1s edges by using the sharp 2p-to-3d transition in TiO_2 (rutile), as in previous work.[33] The generation of N_2 trapped in the bulk of the sample allows for its use as a calibration standard.[34] The first vibrational line of N_2 at 400.9 eV (ref 35) was used for calibration of the fluorescence yield (FY) N 1s spectra. The absolute accuracy is about ±0.2 eV; the relative accuracy between different compounds, about ±0.1 eV; and the relative accuracy between different π^* peaks at the same absorption edge, about ±0.05 eV. The energy resolution was significantly better than the width of the observed features, with the vibrational splitting of N_2 at the N 1s edge clearly resolved.

The radiation dose (in Gy = J/kg) is determined as in previous work[33] by the following formula:

$$\text{Dose} = \left(\frac{I \cdot t}{Y_{Au}}\right)\left(\frac{1-F}{F}\right)\left(\frac{E}{V \cdot \rho}\right)$$

I is the photocurrent from the Au mesh; t is the exposure time; Y_{Au} is the photoelectric yield of Au, which is taken to be 10% at ~400 eV and 11% at ~550 eV (ref 36); F is the fraction of photons intercepted by the mesh (~10%); E is the energy per photon; V is the irradiated volume of the sample; and ρ is the density of the sample. For PMDI, the volume is 1.4 $mm^2 \cdot 0.4$ μm (spot size times absorption length). For SSMCC, the volume is 1 $mm^2 \cdot 0.4$ μm. The density of each compound is assumed to be 1.35 g/cm^3 by comparison with similar compounds.[37] The absorption length is estimated as the length at which the transmittance of the sample for 400 eV photons decreases by a factor of e, using the Center for X-ray Optics database[38] and calculator.[39]

RESULTS AND DISCUSSION

X-ray Absorption Spectra. Figure 1 shows the N 1s absorption edge TEY spectra of PMDI and SSMCC at increasing levels of exposure to soft X-rays of about 390 eV.

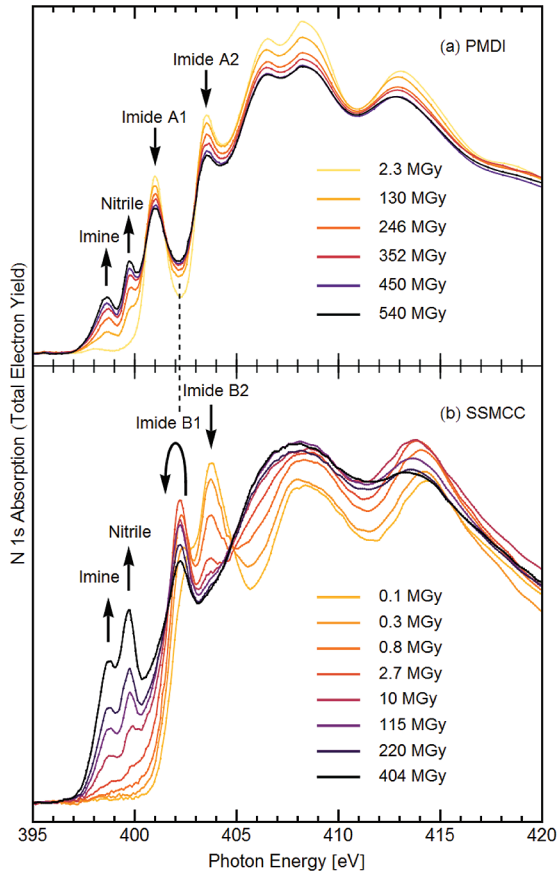

Figure 1. Irradiation-dependent N 1s absorption spectra of (a) PMDI and (b) SSMCC with total electron yield detection. Arrows indicate changes in the peak height with increasing radiation dose. The peak at 402.3 eV in SSMCC initially increases and then decreases in intensity, indicating conversion of imide B2 to imide B1 with subsequent conversion to imine and nitrile. For PMDI, the peaks labeled imide A1 and imide A2 are different orbitals of the same imide.

dx.doi.org/10.1021/jp3003596 | J. Phys. Chem. B 2012, 116, 7048–7054

These TEY spectra were taken at the U2 VLS-PGM beamline at the Synchrotron Radiation Center (SRC) as described previously.[33] Two π^* peaks are present in the pristine PMDI spectra (Figure 1a) at 401.0 and 403.4 eV. Because the nitrogens in PMDI are identical, these peaks must correspond to different π^* orbitals[10] of the same imide. As the sample is irradiated, these peaks as well as the σ^* region decrease in intensity, while the post-edge region remains relatively constant. Simultaneously, peaks rise at 398.6 and 399.7 eV, corresponding to imine and nitrile bonds, respectively. This indicates that the radiation damage mechanism of imides is similar to that of amides. No significant nitrogen is lost from the molecule, but bonds are rearranged in such a way as to form imines and nitriles. The spectra seen in Figure 1 were low-dose analytical spectra taken between high-dose exposures at 388 eV.

Two distinct imides are present in SSMCC. These give rise to distinct π^* peaks in Figure 1b. The peak at 403.7 eV, attributed to imide B2, disappears rapidly with irradiation, in contrast to the peak at the same energy in PMDI, which remains visible, even at much higher total exposure. As imide B2 decreases, the lower energy peak at 402.1 eV (attributed to imide B1) grows, suggesting a conversion of imide B2 to imide B1 as a first step of the radiation damage process. When the imide B2 peak disappears, the imide B1 peak's growth stops, and it begins to decay. Simultaneously, imine and nitrile π^* peaks appear, as in PMDI and amides. Thus, the photodissociation of SSMCC contains a more complex consecutive reaction, in which imide B2 is first converted to an imide similar to imide B1 before being converted into imines and nitriles.

Table 2. N 1s → π^* Transition Energies and Assignments for PMDI

	TEY energy [eV]	assignment
1	398.6	imine
2	399.7	nitrile
3	401.0	imide A1
4	403.4	imide A2

Table 3. N 1s → π^* Transition Energies and Assignments for SSMCC

	TEY energy [eV]	FY energy [eV]	assignment
1	398.6	398.7	imine
2	399.7	399.8	nitrile
3		400.9	N_2 (ν = 0)
4		401.1	N_2 (ν = 1)
5		401.3	N_2 (ν = 2)
6		401.6	N_2 (ν = 3)
7	402.1	402.3	imide B1
8	403.5		imide B2

The difference in total radiation exposure between the two samples is particularly noteworthy. The PMDI requires a substantially greater dose than the SSMCC to show similar spectral signs of damage. This is not unexpected, as aromatic polyimides are known to be stable.[3,5] SSMCC, however, is less stable due to its reactive maleimide and succinimide groups, a property useful for its applications as a linker for attaching biological samples to substrates.[7,8] As a result, one expects that the more stable of the two imide structures in the SSMCC spectrum would be more similar to the imide structure in PMDI. This suggests the assignment of the maleimide in SSMCC as imide B1 and the succinimide as imide B2. Diacetimide, which does not have a ring structure, shows a single π^* peak at an energy similar to that of the peak assigned to imide B2 in Figure 1, further supporting the assignment of the succinimidyl imide as imide B2.[40] The higher energy of the imide B2 peak compared with diacetimide is likely due to a shift in the N 1s binding energy caused by the nearby oxygens bonded to the succinimidyl nitrogen.

There is another possible explanation for the assignment of the two imide π^* peaks in Figure 1b, in which the assignments of the peaks to imide B1 and imide B2 are interchanged. It is less convincing but cannot be ruled out completely. In that case, the imide B1 π^* orbital splits into two orbitals the same way as in PMDI, as both are coupled to an aromatic π system. The upper peak in SSMCC (labeled imide B2 in Figure 1) would be equivalent to the upper peak in PMDI, while the lower peak in PMDI would be hidden in the low-energy tail of the peak labeled imide B1. Imide B2 would have a single π^* peak at the position labeled imide B1. Since imide B2 does not couple to an aromatic π^* system, one would, indeed, expect only a single π^* peak, which should be located near the center of gravity of the split π^* manifold of PMDI, as indicated by a vertical dashed line in Figure 1. However, such an assignment would suggest that the upper π^* peak of SSMCC should be less sensitive to irradiation than the lower peak, since PMDI with its aromatic coupling is much less sensitive than SSMCC.

FY and TEY spectra were measured simultaneously in successive scans at beamline 8.0 at the Advanced Light Source (ALS) using a channelplate detector with an Al filter for the FY. This makes it possible to detect both the surface region (with an escape depth of ~5 nm for secondary electrons) using TEY measurements and the bulk (with an absorption length of 350 nm just below the N 1s edge) using FY measurements. Figure 2a shows the FY spectra of SSMCC as the total radiation dose increases. The TEY spectra taken simultaneously are also shown and are consistent with the spectra in Figure 1 at a comparable dose.

Two major differences between the TEY and FY spectra of SSMCC are immediately apparent. First, the imide B2 peak is not present in the FY spectra. This is most likely because the greater intensity at the ALS had already sufficiently damaged the sample to the point that the majority of the imide B2 had been converted into imide B1, imine, or nitrile. Second, a strong peak rises with vibrational fine structure at 400.9, 401.1, 401.3, and 401.6 eV. These energies are fingerprints of the π^* transition of the N_2 molecule.[35,41] The growth of these peaks indicates formation of N_2 as one of the radiation damage products, which is subsequently trapped in the bulk of the sample. The absence of the N_2 peaks from the TEY spectra is due to TEY only probing the surface region of the sample. Any N_2 formed on the surface would desorb and thus not appear in TEY spectra. A similar evolution of N_2 was observed after irradiation of ammonium salts[34,42] and frozen ammonia.[43] The FY spectra otherwise match the higher exposure TEY spectra. The imide B1 π^* peak decays with increasing radiation dose while the imine, nitrile, and N_2 π^* peaks grow.

The O 1s absorption edge also provides insight on the processes occurring in the irradiation of PMDI and SSMCC. Figure 3a shows O 1s absorption edge TEY spectra for PMDI, taken in low-dose analytical scans between periods of high dose exposure at 388 eV. An overall decrease in intensity at all energies can be seen, indicating a loss of oxygen without any significant change in how the oxygen is bonded, as in the amide

dx.doi.org/10.1021/jp3003596 | J. Phys. Chem. B 2012, 116, 7048−7054

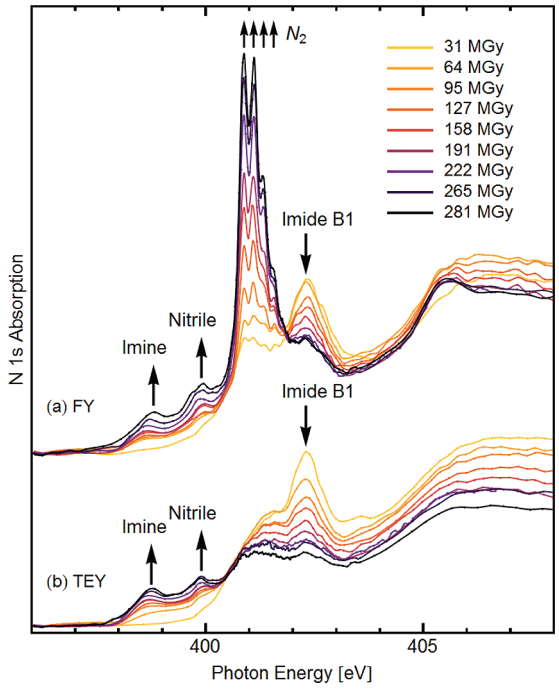

Figure 2. Irradiation-dependent N 1s absorption spectra of SSMCC with (a) fluorescence and (b) total electron yield detection, taken simultaneously on the same sample. Arrows indicate changes with increasing radiation dose. Comparing the two, an additional set of peaks with the vibrational fine structure of N_2 is observed in the fluorescence yield data. N_2 becomes trapped inside the film and is accessible only with the deeper penetration of fluorescence photons.

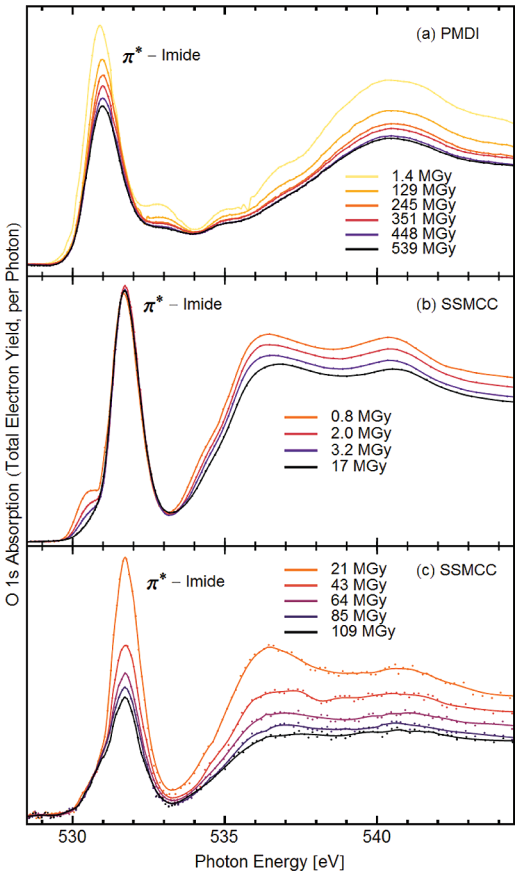

Figure 3. Irradiation-dependent O 1s absorption spectra of (a) PMDI and (b, c) SSMCC, with b for low and c for high exposure (electron detection). A low-energy shoulder of the dominant imide π^* peak in the SSMCC spectra rapidly quenches at low dose. With higher doses, there is an intensity loss of all spectral features, indicating loss of oxygen.

radiation damage process.[33] Figure 3b and c show O 1s absorption edge TEY spectra for SSMCC in low- and high-dose regimes, respectively, taken in successive scans. Next to the strong imide carbonyl π^* at 531.7 eV, a low-energy shoulder visible in the low-dose spectra rapidly quenches as the dose increases and is absent in the high-dose spectra. Both sets of spectra show an overall decrease in intensity at all energies, as in PMDI, indicating a loss of oxygen without any significant change in how the oxygen is bonded, as in the amide radiation damage process.[33] By comparison with the N 1s spectra, we attribute the lower energy shoulder to the N−O bond in imide 2 due to its rapid quenching.

Peak Intensity versus Exposure. To analyze the changes in SSMCC with increasing radiation dose, we have fit the curves in each of the TEY N 1s absorption spectra for PMDI and SSMCC according to established procedures. We limit our analysis to the π^* region of the spectra because it has clearer structure and provides more information about the changes in bonding in the molecule. Tracking the changes in intensity of the fit peaks as radiation dose increases allows the creation of reaction curves analogous to chemical reaction rate curves. Fitting to this data using reaction rate equations[44] then gives insight into the steps in the radiation damage process in terms of which bonds are converted to which.

An example fit to one of the TEY spectra of SSMCC is shown in Figure 4. All peaks are Gaussian, and the background is approximated by adding the σ^* peak and the integral of each π^* peak to the spectrum, with a scaling factor. Some asymmetry is present in some of the peaks (particularly the imide B1 peak in the SSMCC spectra), which is compensated for by scaling the fit peaks such that the areas of the fit curve's (blue curve in

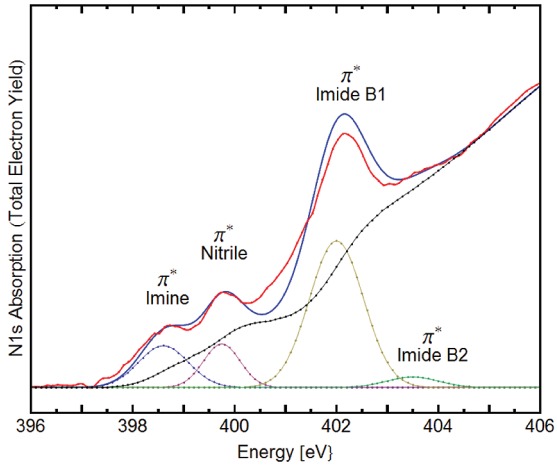

Figure 4. A fit to an SSMCC spectrum at an exposure of 20 MGy (compare Figure 1). The red curve represents the experimental data, and the blue curve, the fit. The black background curve consists of integrals of the peaks plus a broad peak near 408 eV representing the continuum of σ^* transitions. The asymmetric imide B1 peak does not match the symmetric line shape used here, but the deviation in the peak areas was minimized by having equal amounts of overshoot and undershoot.

dx.doi.org/10.1021/jp3003596 | J. Phys. Chem. B 2012, 116, 7048−7054

Figure 4) deviations from the data (red curve in Figure 4) approximately cancel. The asymmetry in the spectra (particularly in the imide B1 peak of the SSMCC spectra) might be explained by the desorption of reaction products, such as N_2, exposing fresh imide; that is, imide B1 (and to a smaller degree imide B2) never vanishes completely at high exposures.

Modeling by Rate Equations. Figure 5 shows intensity versus exposure plots for the peaks in the TEY spectra. The data are normalized such that the areas of the pristine imide A1 peak in PMDI and the pristine imide B2 peak in SSMCC are ~1. This normalization makes the area of the imide B1 peak in SSMCC also ~1, as would be expected, given that each SSMCC molecule contains one of each type of imide. The small discrepancy is due to differences in absorption cross sections. The x-scale is linear in Figure 5a and logarithmic in b. The PMDI reaction curves can be fit with simple first-order reaction rate equations,[44] which is consistent with a process of breaking up the imides into imines and nitriles. The TEY reaction curves for SSMCC may be fit reasonably well with rate

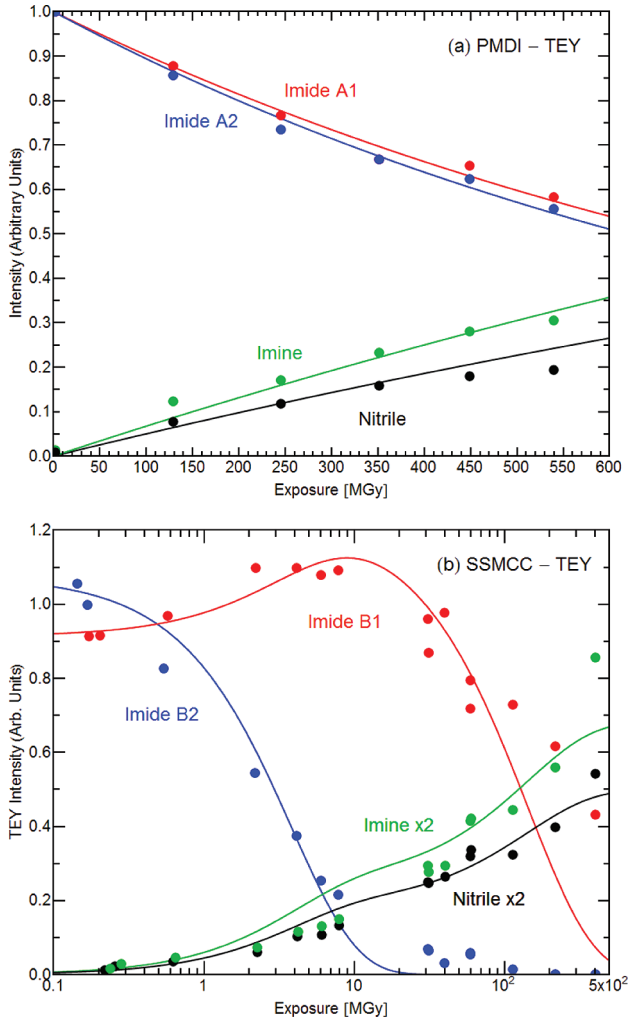

Figure 5. Areas of the π^* peaks versus exposure for (a) PMDI (Table 2) and (b) SSMCC (Table 3), taken with electron detection (Figure 1). For SSMCC, the imine and nitrile data have been magnified by a factor of 2. The curves are the results of the rate eqs (1−3) They provide reaction constants and cross section ratios (listed in the Supporting Information).

equations for a more complicated set of consecutive and parallel reactions.

The reaction scheme for PMDI is that of two parallel first-order reactions, imide → imine and imide → nitrile. The first-order reaction rate equations used to fit the PMDI decay curves are derived from the following differential equations:

$$\frac{dn_A}{dx} = -k_1 n_A - k_2 n_A \quad (1)$$

$$\frac{dn_B}{dx} = k_1 n_A \quad (2)$$

$$\frac{dn_C}{dx} = k_2 n_A \quad (3)$$

n_A is the imide number density; n_B is the imine number density; n_C is the nitrile number density; k_1 is the rate constant for the decay from imide to imine; k_2 is the rate constant for the decay from imide to nitrile; and x is the total exposure in MGy. The number density of an orbital can be defined as

$$n_i \equiv \frac{I_i}{\sigma_i} \quad (4)$$

I_i is the area of the spectral peak for that orbital (which is the measurable quantity in the spectra), and σ_i is the absorption cross-section. Replacing the n_i's using this definition and solving for the I_i's then gives equations that can be used to fit the peak areas as a function of dose (see Supporting Information for the rate equations and parameters).

The rate equations and reaction scheme for the SSMCC spectra are more complicated due to the two inequivalent imides B1 and B2 (see Table 1). The reaction scheme is a combination of consecutive and parallel reactions: imide B2 → imide B1, imide B2 → imine, imide B2 → nitrile, imide B1 → imine, and imide B1 → nitrile. This scheme yields the following differential equations:

$$\frac{dn_A}{dx} = -k_1 n_A - k_2 n_A - k_3 n_A \quad (5)$$

$$\frac{dn_B}{dx} = k_1 n_A - k_4 n_B - k_5 n_B \quad (6)$$

$$\frac{dn_C}{dx} = k_2 n_A + k_4 n_B \quad (7)$$

$$\frac{dn_D}{dx} = k_3 n_A + k_5 n_B \quad (8)$$

n_A is the number density of the imide B2 orbital; n_B is the number density of the imide B1 orbital; n_C is the number density of the imine orbital; n_D is the number density of the nitrile orbital; k_1 is the rate constant for the decay from imide B2 to imide B1; k_2 is the rate constant for the decay from imide B2 to imine; k_3 is the rate constant for the decay from imide B2 to nitrile; k_4 is the rate constant for the decay from imide B1 to imine; k_5 is the rate constant for the decay from imide B1 to nitrile; and x is the total exposure in MGy. The definition in eq 4 again applies, so the number densities can be replaced by peak areas and cross sections. Note that the number densities for imides B1 and B2 before irradiation should be identical; that is, $n_A^0 = n_B^0$. This gives us the extra condition that $\sigma_B/\sigma_A = I_B^0/I_A^0$. Solving these differential equations gives the rate equations for imide B2, imide B1, imine, and nitrile, which are rate equations

dx.doi.org/10.1021/jp3003596 | J. Phys. Chem. B 2012, 116, 7048−7054

for consecutive and parallel first-order reactions. For examples of such rate curves of these types of reactions, see Figures 3-2 and 3-3 in ref 44. For the rate equations and parameters for SSMCC, derived the same way as for PMDI, see the Supporting Information.

Table 4. Rate Constants for PMDI and SSMCC Rate Equations

molecule	rate constant	value [MGy^{-1}]
PMDI	k_1	5.1×10^{-4}
	k_2	5.1×10^{-4}
SSMCC	k_1	8.8×10^{-2}
	k_2	8.6×10^{-2}
	k_3	8.6×10^{-2}
	k_4	3.5×10^{-2}
	k_5	3.5×10^{-2}

From the fit to the rate equations in Figure 5, we obtain the rate constants for the various reactions. These results are listed in the Supporting Information. Most notably, we find that imide B2 is converted rather rapidly into imide B1, which leads to the peak in the intensity of imide B1 before both decay more slowly into imine and nitrile. The height of this peak is sensitive to the ratio of the reaction constants k_1, k_A, and k_B, where $k_A = k_1 + k_2 + k_3$ and $k_B = k_4 + k_5$. The maximum height is the sum of the pristine intensities of imides B1 and B2, which is reached in the limit of very fast conversion of imide B2 to B1 (before imide B1 has time to decay). The excess of imide B2 at the end of the calculated decay curve can be attributed to the desorption of reaction products, which keeps exposing pristine imide. An example is the formation of N_2, which can be observed in the bulk, but not at the surface, where N_2 desorbs into the vacuum chamber. The desorption of N_2 also is likely responsible for the reduction in the overall area of the π^* region at the N 1s edge (see Figure 1). The fit to the imine and nitrile reaction products will be affected if there is a further reaction that removes imine and nitrile, such as desorption or N_2 formation. Such an effect would make the cross section of imine and nitrile appear smaller than it actually is.

There are a few caveats to the use of the intensity curves in Figure 5. Each data point is the area under a peak, rather than the concentration of a molecule. The peak areas are given by the product of the concentration and the photoabsorption cross section for a specific molecular orbital. This explains why imides B1 and B2 have slightly different intensities at zero exposure in Figure 5b and c, despite SSMCC containing one each of imide B1 and imide B2. When comparing TEY and FY measurements, one needs to realize that TEY data are surface-sensitive (5−10 nm), whereas the FY measurements reflect the bulk (100 nm−1 μm). An additional process not considered in the rate equations is the desorption of reaction products. It exposes undamaged molecules. This effect prevents the data points for imide B2 from coming down all the way to zero at high exposure in Figure 5.

CONCLUSIONS

This work explores dissociation mechanisms for imides, starting with a simple molecule (PMDI) and moving on to a more complex molecule (SSMCC) containing different imides with different reactions. In PMDI, the imide is converted to imine and nitrile in a process similar to that seen in radiation-induced decay of amides.[33] In SSMCC, one of the two imides is initially converted to the other before both react into imine and nitrile after desorption of oxygen. In addition, molecular N_2 is formed and remains trapped inside the sample. These processes are inferred from bulk- and surface-sensitive N 1s spectra, which are modeled by reaction rate equations. They are compared with recently proposed photodissociation processes for amides[33] and amino acids.[17] All three processes lead to imine plus nitrile as reaction products. It is quite possible that the eventual formation of N_2 observed here for SSMCC occurs for amides, as well.

These results demonstrate how a rather complex photodissociation process may be unraveled via element- and bond-specific spectroscopy. Simultaneous investigation of the surface and bulk of a sample using electron detection and fluorescence detection allows X-ray absorption spectroscopy to distinguish volatile from permanent products. It would be interesting to determine the limits of this method in terms of complexity of molecular structure and number of reaction steps as well as to identify the factors influencing the branching ratio between imine and nitrile reaction products and the generation of N_2.

ASSOCIATED CONTENT

Supporting Information

Integrated rate equations, constraints, and parameters used for fitting the reaction curves in Figure 5. This material is available free of charge via the Internet at http://pubs.acs.org.

AUTHOR INFORMATION

Corresponding Author

*E-mail: fhimpsel@wisc.edu

Notes

The authors declare no competing financial interest.

ACKNOWLEDGMENTS

This work was supported by the NSF under awards DMR-1121288 (MRSEC) and DMR-0537588 (SRC) and by the DOE under Contracts Nos. DE-FG02-01ER45917 (end station) and DE-AC02-05CH11231 (ALS).

REFERENCES

(1) Li, R.; Li, C.; He, S.; Di, M.; Yang, D. *Radiat. Phys. Chem.* **2008**, *77*, 482−489.
(2) Sun, C.; Wu, Y.; Xiao, J.; Li, R.; Yang, D.; He, S. *J. Appl. Phys.* **2011**, *110*, 124909.
(3) Kang, P.-H.; Jeon, Y.-K.; Jeun, J.-P.; Shin, J.-W.; Nho, Y.-C. *J. Ind. Eng. Chem.* **2008**, *14*, 672−675.
(4) Ghosh, S.; Klett, R.; Fink, D.; Dwivedi, K.; Vacík, J.; Hnatowicz, V.; Červena. *J. Radiat. Phys. Chem.* **1999**, *55*, 271−284.
(5) Megusar, J. *J. Nucl. Mater.* **1997**, *245*, 185−190.
(6) Harada, K.; Fujitsuka, M.; Sugimoto, A.; Majima, T. *J. Phys. Chem. A* **2007**, *111*, 11430−11436.
(7) Bai, Y.; Liu, X.; Cook, P.; Abbott, N. L.; Himpsel, F. J. *Langmuir* **2010**, *26*, 6464−6470.
(8) Leonard, D. N.; Franzen, S. *J. Phys. Chem. C* **2009**, *113*, 12706−12714.
(9) Zhang, H.; Xu, X.; Ji, H.-F. *Chem. Commun.* **2010**, *46*, 1917−1919.
(10) Wakita, J.; Sekino, H.; Sakai, K.; Urano, Y.; Ando, S. *J. Phys. Chem. B* **2009**, *113*, 15212−15224.
(11) Von Sonntag, J.; Knolle, W.; Naumov, S.; Mehnert, R. *Chem.—Eur. J.* **2002**, *8*, 4199−4209.
(12) Itälä, E.; Ha, D.; Kooser, K.; Huels, M.; Rachlew, E.; Nõmmiste, E.; Joost, U.; Kukk, E. *J. Electron Spectrosc. Relat. Phenom.* **2011**, *184*, 119−124.

(13) Samant, M. G.; Stöhr, J.; Brown, H. R.; Russell, T. P.; Sands, J. M.; Kumar, S. K. *Macromolecules* **1996**, *29*, 8334−8342.
(14) Zharnikov, M.; Ouchi, Y.; Hasegawa, M.; Scholl, A. *J. Phys. Chem. B* **2004**, *108*, 859−863.
(15) Ruiz-Osés, M.; Kampen, T.; González-Lakunza, N.; Silanes, I.; Schmidt-Weber, P. M.; Gourdon, A.; Arnau, A.; Horn, K.; Ortega, J. E. *ChemPhysChem* **2007**, *8*, 1722−1726.
(16) Zubavichus, Y.; Fuchs, O.; Weinhardt, L.; Heske, C.; Umbach, E.; Denlinger, J. D.; Grunze, M. *Radiat. Res.* **2004**, *161*, 346−358.
(17) Wilks, R. G.; MacNaughton, J. B.; Kraatz, H.-B.; Regier, T.; Blyth, R. I. R.; Moewes, A. *J. Phys. Chem. A* **2009**, *113*, 5360−5366.
(18) Coffey, T.; Urquhart, S. G.; Ade, H. *J. Electron Spectrosc. Relat. Phenom.* **2002**, *122*, 65−78.
(19) Beetz, T.; Jacobsen, C. *J. Synchrotron Radiat.* **2003**, *10*, 280−283.
(20) Wang, J.; Morin, C.; Li, L.; Hitchcock, A.; Scholl, A.; Doran, A. *J. Electron Spectrosc. Relat. Phenom.* **2009**, *170*, 25−36.
(21) Alizadeh, E.; Gschliesser, D.; Bartl, P.; Hager, M.; Edtbauer, A.; Vizcaino, V.; Mauracher, A.; Probst, M.; Märk, T. D.; Ptasińska, S.; Mason, N. J.; Denifl, M.; Scheier, P. *J. Chem. Phys.* **2011**, *134*, 054305.
(22) Lucas, B.; Grégoire, G.; Lemaire, J.; Maître, P.; Ortega, J.-M.; Rupenyan, A.; Reimann, B.; Schermann, J. P.; Desfrançois, C. *Phys. Chem. Chem. Phys.* **2004**, *6*, 2659−2663.
(23) Laskin, J.; Denisov, E.; Futrell, J. *J. Am. Chem. Soc.* **2000**, *122*, 9703−9714.
(24) Polce, M. J.; Ren, D.; Wesdemiotis, C. *J. Mass Spectrom.* **2000**, *35*, 1391−1398.
(25) Rogalewicz, F.; Hoppilliard, Y.; Ohanessian, G. *Int. J. Mass Spectrom.* **2000**, *195*−*196*, 565−590.
(26) Laskin, J.; Futrell, J. H. *J. Chem. Phys.* **2002**, *116*, 4302−4310.
(27) Wang, J.; Meroueh, S. O.; Wang, Y.; Hase, W. L. *Int. J. Mass Spectrom.* **2003**, *230*, 57−63.
(28) Nielsen, S. B.; Andersen, J. U.; Hvelplund, P.; Liu, B.; Tomita, S. *J. Phys. B: At., Mol., Opt. Phys.* **2004**, *37*, R25.
(29) Fenn, J. B.; Mann, M.; Meng, C. K.; Wong, S. F.; Whitehouse, C. M. *Science* **1989**, *246*, 64−71.
(30) Karas, M.; Hillenkamp, F. *Anal. Chem.* **1988**, *60*, 2299−2301.
(31) Karas, M.; Bahr, U.; Fournier, I.; Glückmann, M.; Pfenninger, A. *Int. J. Mass Spectrom.* **2003**, *226*, 239−248.
(32) Wind, M.; Lehmann, W. D. J. *Anal. At. Spectrom.* **2004**, *19*, 20−25.
(33) Johnson, P. S.; Cook, P. L.; Liu, X.; Yang, W.; Bai, Y.; Abbott, N. L.; Himpsel, F. J. *J. Chem. Phys.* **2011**, *135*, 044702.
(34) Gillespie, A. W.; Walley, F. L.; Farrell, R. E.; Regier, T. Z.; Blyth, R. I. R. *J. Synchrotron Radiat.* **2008**, *15*, 532−534.
(35) Sodhi, R. N. S.; Brion, C. E. *J. Electron Spectrosc. Relat. Phenom.* **1984**, *34*, 363−372.
(36) Henke, B. L.; Knauer, J. P.; Premaratne, K. *J. Appl. Phys.* **1981**, *52*, 1509−1520.
(37) Fischer, H.; Polikarpov, I.; Craievich, A. F. *Protein Sci.* **2004**, *13*, 2825−2828.
(38) Henke, B.; Gullikson, E.; Davis, J. *At. Data Nucl. Data Tables* **1993**, *54*, 181−342.
(39) Gullikson, E. Center for X-Ray Optics, X-Ray Interactions With Matter; 2010; http://henke.lbl.gov/optical_constants/
(40) Lessard, R.; Cuny, J.; Cooper, G.; Hitchcock, A. P. *Chem. Phys.* **2007**, *331*, 289−303.
(41) Schwarzkopf, O.; Borchert, M.; Eggenstein, F.; Flechsig, U.; Kalus, C.; Lammert, H.; Menthel, U.; Pietsch, M.; Reichardt, G.; Rotter, P.; Senf, F.; Zeschke, T.; Peatman, W. B. *J. Electron Spectrosc. Relat. Phenom.* **1999**, *101*−*103*, 997−1001.
(42) Aziz, E. F.; Gråsjö, J.; Forsberg, J.; Andersson, E.; Söderström, J.; Duda, L.; Zhang, W.; Yang, J.; Eisebitt, S.; Bergström, C.; Luo, Y.; Nordgren, J.; Eberhardt, W; Rubensson, J. E. *J. Phys. Chem. A* **2007**, *111*, 9662−9669.
(43) Parent, P.; Bournel, F.; Lasne, J.; Lacombe, S.; Strazzulla, G.; Gardonio, S.; Lizzit, S.; Kappler, J.-P.; Joly, L.; Laffon, C.; Carniato, S. *J. Chem. Phys.* **2009**, *131*, 154308.
(44) Connors, K. A. *Chemical Kinetics, The Study of Reaction Rates in Solution*; VCH, New York, 1990.